SPE 99520

Gas Storage and Operations in Single Bedded Salt Caverns: Stability Analyses

Gang Han, Mike Bruno, Khang Lao, Jean Young, Terralog Technologies USA, Inc; Luis Dorfmann, Tufts University

This paper was prepared for presentation at the 2006 SPE Gas Technology Symposium held in Calgary, Alberta, Canada, 15–17 May 2006.

Abstract

Bedded salt formations are located throughout the United States, providing valuable storage capacity for natural gas and other hydrocarbons. In order to increase gas storage capabilities and provide operators with improved geotechnical design and operating guidelines for these caverns, stability analyses of single bedded salt cavern have been completed and are described in this paper. This work is a part of integrated efforts initiated and sponsored by the US Department of Energy, Gas Technology Institute, and Pipeline Research Council International, Inc.

Numerical geomechanical models have been developed to investigate single cavern deformation and bedding plane slip for a variety of cavern configurations. A viscoplastic salt model has been developed based on an empirical creep law developed for the Waste Isolation Pilot Plant (WIPP) Program and combined with a Drucker-Prager model for damage and failure. The non-salt materials are described with either a traditional Mohr-Coulomb model, or an elastic model, depending on layer properties.

A baseline model with specified geometric dimensions is first selected and subjected to one year cyclic pressure operations. The amount of damage around the cavern wall and roof is evaluated and used as a comparison in the study. Then the operations are extended to 15 years to study cavern stability for long term gas storage and operations. In addition to the baseline model, parametric studies have been performed to investigate cavern damage as a function of salt roof thickness, overburden stiffness, interface properties, and cavern geometries. Each cavern simulation includes one year of pressure cycling with a minimum, mean, and maximum cavern pressure of 6.1 MPa (884.5 psi), 8.8 MPa (1276 psi) and 14.9 MPa (2160.5 psi), respectively. Different operation conditions, e.g. hydrostatic, cyclic, and a direct pressure drawdown, are compared and evaluated in terms of cavern stability.

These analyses can serve as a basis to select the best salt cavern candidate for gas storage and operations. They can also help to assess critical cavern design parameters for thin bedded salt formations.

Introduction

The US Depart. Of Energy (DOE) forecasts global natural gas consumption increasing nearly 70% between 2002 and 2025, with the strongest growth coming from Asia, Eastern Europe, and the former Soviet Union[1]. This poses significant challenges to gas reservoir development, gas transportation, and storage. Currently there are three main types of natural underground storage facilities for natural gas: depleted reservoirs, aquifers, and salt caverns. Salt caverns are typically much smaller than depleted reservoirs and aquifers, and therefore they hold much less gas volume. In 2001, the US total gas storage capacity was about $2.38\times10^{11}m^3$ (8.4tcf), 82% of which was stored in depleted gas reservoirs, 15% in aquifers, and 3% in salt caverns[2]. Despite the fact that deplete reservoirs are the dominant storage method for natural gas, it is estimated that salt caverns represent 15% of daily deliverability (a measure of the amount of gas that can be withdrawn from a storage facility) in the US[2]. Salt caverns storage hold the advantages related to higher deliverability, lower cushion (or base) gas requirement, less development cost, faster to initiate the gas flow, and quicker to refill.

There are two types of underground salt deposits: salt domes and bedded salts. Bedded salts are the primary focus in this study because they are shallower and thinner formations than natural salt domes, and therefore more prone to stability risks during gas extraction and injection. Bedded salt formations are found in several areas throughout the United States and Canada[3,4]. The largest basins include the Permian Basin across Texas, Oklahoma, Kansas, Colorado, and New Mexico, the Gulf Coast Basin across Southern Texas, Louisiana, Mississippi, and Alabama, and the Michigan and Appalachian Basins across the states of Michigan, Ohio, Pennsylvania and New York. These areas have experienced different deposition and tectonic history, resulting in some differences in depth, lithology and typical geologic structure for the dominant bedded salt intervals. Bedded salt formations in all these areas, however, are layered and interspersed with non-salt sedimentary materials such as anhydrite, shale, dolomite, and limestone. The “salt” layers themselves also often contain significant impurities.

According to DOE data for 2001[2], each percentage increase of salt cavern storage capacity in the US represents an additional $6.23\times10^{7}m^3$ (2.2 bcf) of storage capacity. However,

there are certain pressure limits over which a bedded salt cavern can operate. Injecting more gas underground creates higher cavern pressure, which may cause tensile fractures in the salt and jeopardize its stability. Too aggressive subtraction from the cavern should also be avoided because of the concern over roof instability, excessive closures, or even cavern collapse. Furthermore, the decline or increase of cavern pressure may trigger bedding plane slip between heterogeneous material layers. The creep response of salt, which is a function of the deviatoric stress components, may accelerate cavern closure at low cavern pressure if a hydrostatic state of stress vanishes.

This study focuses on single cavern stability under various operating conditions such as direct drawdown and pressure cycling. We also consider the effect of cavern geometries, overburden stiffness, salt roof thickness, interface properties, etc. The primary objective is to increase the gas storage capabilities by providing operators with improved geotechnical design and operating guidelines for thin bedded salt caverns (e.g. maximum and minimum cavern pressure, direct or cyclic pressure draw down, etc). This work forms part of the integrated efforts initiated and sponsored by the Technology Institute, The US Department of Energy, and the Pipeline Research Council International.

Modeling Efforts

The geomechanical analyses are performed with the aid of a commercial numerical stress code, FLAC3D[5]. Four different formation layers are included: clastic, anhydrite, salt, and presalt (see Figure 4). Non-salt rock formations are modeled with a Mohr-Coulomb type of material model. The salt is modeled with a modified creep viscoplastic model combining the WIPP (Waste Isolation Pilot Plant) model and the Drucker-Prager failure model, which includes the initiation of damage, volumetric dilation and ultimate failure. With appropriate boundary conditions applied, salt cavern stability is first studied under cyclic pressure conditions. This also serves as a baseline study, wherein stress, deformation, and rock damage are then compared to various situations, such as different pressure operations, cavern size and geometry, cavern roof thickness, overburden stiffness, properties of layer interface, etc. The details of the testing matrix are listed in Table 3. Based on these analyses, maximum and minimum cavern pressures are estimated, under which salt caverns can operate without risk of fracture or collapse.

Constitutive Models for Salt and other Rocks

Designing bedded salt caverns for natural gas and liquid storage must take into account the natural bedded salt mechanical properties, as well as the non-salt strata natural mechanical properties encountered. Geomechanical properties of the four formations, i.e. clastic, anhydrite, salt, and presalt, are summarized in Table 3. The non-salt materials are described with a traditional Mohr-Coulomb model while the anhydrite layer, immediately above the salt formation, has strain-softening behavior. The data is adapted from the mechanical properties of nonsalt material in the Permian Basin[6].

It is known that the elastic and thermal properties of salt do not change significantly from site to site[7]. However, salt inelastic deformation, creep properties, and damage behaviours can vary dramatically between sites[8]. In-situ stresses, moisture content, fabric anisotropy (crystal imbrications or elongation, and temperature influence the mechanical behaviour of salt. The rate of salt deformation is primarily controlled by the stress difference and the temperature. The stress in the salt outside the cavern depends on the weight of the overburden. The pressure inside the cavern is equal to the weight of fluid or the operating gas pressure. Therefore cavern deformation, creep, and salt damage risk increase with depth, due to both increasing stress and temperature, and with larger differences between the internal cavern pressure and the external in-situ stresses. Moreover, the fact that salt creeps and deforms differently than typical rocks in heterogeneous layers indicates that the salt will expand but the other non-salt layers will not, thereby shear stresses and bedding plane slips may develop.

The salt is described by a modified WIPP-creep viscoplastic model, which includes the WIPP-creep model and Drucker-Prager failure criteria. Figure 2 shows the creep response of a Permian salt at 100°C and is compared with published experimental data[6]. Salt response is characterized by three important types of behavior: initial elastic response followed by damage accumulation, dilation, and eventually failure, the transient creep, and the steady-state creep rate. Damage accumulation during primary loading is achieved by introducing a deformation dependent shear modulus G, which depends nonlinearly on the second deviatoric stress invariant. A change in the shear modulus induces a change in the volumetric response as well. The volumetric dilation and eventual material failure are based on Drucker-Prager failure criteria. The details of creep calculations are described as a part of WIPP model[5]. Experimental data of the Permian salt also shows that during unloading and subsequent reloading, the material response is determined by initial undamaged stiffness properties. This characteristic was implemented as well and is essential to study cyclic loading. The parameters used in the salt model are listed in Table 2.

Model Geometries and Boundary Conditions

Based on the cavern geometries surveyed in the Permian, Michigan and Appalachian Basins, an axisymmetric layout in geology and loading conditions is assumed (Figure 3). This allowed us to model a 3D wedge portion of the cavern and surrounding formation, rather than the full diameter. The geometric layout of the model is a cylindrical shaped cavern 30 m in height and 60 m in diameter. The cavern main roof is located at the depth of 762 m below the free surface. The cavern itself is located in the center of a 54 m thick salt layer, which is covered by a 5 m thick anhydrite layer. The thickness of the salt layer was increased to 78 m to investigate the cavern response when the cavern roof is increased to twice the thickness. A frictional slip interface is located between the anhydrite layer and the salt to study interface slippage. Similarly, a second slip interface is located between the salt and the underlining pre-salt material, see Figure 4. The salt temperature was not considered as a design variable and kept constant at 31 degree Celsius.

A vertical stress is applied consistent with the density of overlying sediments, i.e. increasing with depth and equivalent

to $\sigma_v \approx \int \rho g \, dz$. The radial displacement at the outer surface of the model is fixed in order for the horizontal stress to develop in accordance with the vertical load and the proper Poisson ratio for the different lithologic layers.

Baseline Studies of Single Cavern Stability

In the baseline study the cavern is subjected to pressure cycles. The simulation is carried out in the following steps:

1. Define initial geologic layers and initial stress conditions;
2. Excavate cavern, apply a constant internal cavern pressure equal to the hydrostatic pressure of 8.8 MPa (1276 psi) at a depth of approximately 762 m (2500 ft);
3. Allow the model to reach equilibrium and subsequently to creep for 3 months;
4. Apply pressure cycles for the duration of 1 year. As indicated in Figure 5, the cavern pressure oscillates between the minimum pressure (6.1 MPa, or 884.5 psi) and maximum pressure (14.9 MPa, or 2160.5 psi); and,
5. For each simulation, we evaluate rock stresses and deformation, the development of damage defined as the formation of micro-cracks, as well as possible bedding plane slip along the two interfaces.

Cavern Stress, Deformation, and Damage at Hydrostatic State. Figure 6 shows the distribution of shear stress σ_{xz} and the interface slip after mechanical equilibrium has been reached. The horizontal axis is indicated by x, the vertical by z. The state of shear stress corresponds to a constant hydrostatic cavern pressure of 8.8MPa (1276psi). Due to long term creep, the salt layer away from the cavern boundaries is in a hydrostatic state of stress, i.e. the horizontal stress in the salt layer is much larger than the corresponding horizontal stress in the anhydrite or in the pre-salt. This difference in horizontal stress must be carried by the two interfaces, which may fail when the stress difference exceeds a limit value. The local interface failure for the baseline case at equilibrium is indicated by circles in Figure 6. Figure 7 illustrates the contour plot of the displacement magnitude for equilibrium with a cavern pressure of 8.8MPa (1276psi). The largest displacement is recorded at the cavern roof at an approximate magnitude of 0.01m (0.0328 ft).

Figure 8 demonstrates the distribution of damage in the salt layer after the model reaches equilibrium with the hydrostatic cavern pressure of 8.8MPa (1276psi). The contour plot indicated by *shear-p* is the location where shear damage has occured in the past, and s*hear-n* indicates the locations where shear damage is currently occuring. Similarly, *slipped in the past* and *slipped now* indicate the location where the interface failed in the past or is failing right now. The highest concentration of micro-cracks is located in close proximity of the vertical cavern wall and extends into the cavern roof. The occurance of shear damage is accompanied by a reduction in the material stiffness, and therefore localization of deformation occurs in these areas. Undamaged salt compacts during loading, salt with shear damage and micro-cracks, on the other hand, may dilate. Figure 8 also shows the weak spot of the two material interfaces. This weakness allows slippage of the adjacent materials to occur. The interface properties in this model depend upon the hydrostatic stress, i.e. the interface strength increases with increasing stress through a constant friction angle of 15 degrees. Therefore, the upper interface is somewhat weaker compared to the interface between the salt and pre-salt layer.

Cavern Stress, Deformation, and Damage after 1-year pressure cycles. After the three month of hydrostatic equilibrium, the 1-year pressure cycles are imposed. The internal cavern pressure is first reduced to a minimum of 6.1MPa (884.5psi). The lower limit of the cavern pressure is the most critical parameter for gas subtraction. Reducing the cavern pressure has the following implications.

- The stress in the salt in the proximity to the cavern is no longer hydrostatic. This implies that additional damage in the form of micro-cracks may occur.
- Salt creep deformation and therefore faster cavern closure may occur due to the increase of deviatoric stress. Additionally, localized tensile stresses may develop in the cavern roof and side wall, resulting in possible tensile fracture and even cavern collapse.
- Stresses in the two interfaces may become lower. Lower interface stress implies a reduction in the interface strength, which leads to more likelihood of interface slippage, and roof collapse.

As indicated in Figures 9-11, the interface slip clearly propagates in the upper and lower interfaces after one year of pressure cycles. Furthermore the shear stress and deformation propagate over a larger area (Figure 9 and Figure 10). Even though the magnitude of the shear stress remains approximately the same (Figure 9), the roof displacement increases slightly after cyclic operations (Figure 10). The largest displacement now occurs along the vertical sidewall. Comparing Figure 8 to Figure 11, however, stress redistribution occurs due to the viscoelastic behavior of salt and no additional micro-cracks are formed in the salt formation after pressure cycles.

Factors Influencing Cavern Stability

Several factors which influence cavern stability are investigated and compared to the results from the baseline studies. These include cavern pressure and operations, cavern size and geometry, roof thickness, overburden stiffness, and interface properties. The details of simulation matrix are listed in Table 3.

Cavern Pressures and Operations. In addition to pressure cycles described above, two additional situations are considered with the primary objective to investigate the effect of different operating conditions on cavern stability. The first case keeps the cavern pressure as a constant of 8.8MPa (1276psi) for 15 years; the second keeps a constant cavern pressure of 4.4 MPa (638 psi) for 1 year.

Figure 12 shows the vertical displacement of the cavern roof due to creep over a 15 year period with constant cavern pressure of 8.8MPa. The units of the vertical displacement are meter and the creep time is given in days. The recording of the creep displacement is initiated after static equilibrium is reached, which is the reason why the curve does not start at the origin. During the 15 year period, cavern roof deforms as much as 0.024m (0.0656ft), double the amount occurred after

hydrostatic equilibrium (0.01m). The creep rate, as expected, reduces with time and approaches a constant secondary creep rate. The roof displacement and, correspondingly, the cavern closure are hereafter associated with salt creep deformation.

Lowering the cavern pressure to 4.4 MPa (638 psi), the formation in the proximity to the cavern is no longer in hydrostatic state. Shear-induced micro-cracks propagate throughout the entire roof and cavern floor and extend substantially in lateral directions (see Figure 13). The calculation of the displacement also confirms that the salt formation adjacent to the cavern has deformed three times larger than the original hydrostatic state. Depending on the extent of the cracks or damage, the formation may fail and the cavern may collapse. This potentiality is amplified by an extended slippage along the two interfaces (circles in Figure 13).

This analysis shows that the most critical operational parameter to cavern stability and roof deformation is the lower pressure limit.

Cavern Size and Geometry. The effect of cavern size and geometry, expressed as a Height/Diameter (H/D) ratio, is investigated next. Cavern diameter varies from 60m (i.e. H/D =1/2 in baseline model) to 120m (i.e. H/D =1/4) and 30m (i.e. H/D = 1/1) while the height of the cavern is kept constant (30 m). One year pressure cycles used in the baseline study are applied to all cases.

Shear damage developed around the cavern with H/D ratio of 1/4 subjected to 1 year pressure cycles are shown in Figure 14. Compared to the results of the baseline case (Figure 11), the micro-cracks in the roof and the floor region are more localized to the cavern tip and also extend over a larger area. Further, the slippage occurred in the interfaces extended further due to the higher deformation at the cavern tip.

When the cavern H/D ratio becomes 1, the damaged region is smaller and involves only the vertical cavern wall after 1-year pressure cycles (Figure 15). Furthermore the formation slippage has only occurred in the upper interface. The smaller magnitude of displacement in this case indicates the cavern appears “stronger” when its size becomes smaller.

Cavern Roof Thickness. In this parametric simulation, the effect of salt roof thickness on the cavern geomechanical behaviors and on the damage development is studied. The roof thickness increases 24 m (80 ft), from 12 m (40 ft) in the baseline study.

The amount of rock damage in the cavern roof with double thickness is shown in Figure 16. The damage is reduced when compared to the baseline case (Figure 11), esp. around the center of the roof. It, however, does not seem to be much reduction in damage along the vertical wall of the cavern. Interface slip is still present on the interface between the salt layer and the anhydrite layer. Also, the calculation of vertical displacement indicates an increase of the deformation in the cavern roof compared to the baseline case while the lateral displacement remains about the same. Thick cavern roof does help improve the cavern stability, esp. around roof center. But this improvement is not significant along the cavern wall, where most damage concentrates.

Overburden Stiffness. In the baseline case we considered a 745m clastic overburden with stiffness properties listed in Table 1. In this simulation, the stiffness of the overburden is reduced by a factor of 10. The amount of damage around the cavern and the development of interface slip are examined. The other parameters remain unchanged in the model and pressure cycling over a one year period is assumed.

Figure 17 describes the regions where shear damage has occurred. In the view of the priority given to this study, we do not consider the damage in the overburden but focus on the regions close to the cavern only. It is interesting to point out that there is tensile failure in the anhydrite layer. This is not unexpected since a substantial part of the overburden weight is now transferred to the stiffer anhydrite and ultimately to the cavern roof. Tensile failure in the anhydrite layer implies an increase in the vertical displacement of the cavern roof, and thus more damage in the salt itself (see Figure 18). Calculations indicates that, when overburden becomes soft, the vertical displacement of the cavern roof increases to as much as 0.14m (0.46ft), from 0.01m (0.0328ft) in the baseline study. Furthermore, the interface slippage between the salt layer and the anhydrite layer now covers the entire cross section of the cavern. This simulation clearly demonstrates that the overburden stiffness is a significant factor in evaluating roof stability of caverns.

Properties of Layer Interface. There are two interfaces implemented in the model to study bedding plane slippage. One is located between the anhydrite layer and the salt; the other is between the salt and the underlining pre-salt formation. As mentioned above, the interface strength depends directly on the pressure generated in the interface, i.e. the slip surface is described by a constant friction angle of 15 degree. The results plotted in Figure 19 are obtained by reducing the interface friction angle from the initial 15 degree to 5 degree. Again, a one year pressure cycling period is considered.

Figure 18 clearly shows the increase of the damaged area where interface slips (both at the upper and the lower interfaces). This extended slip zone implies that the stresses at the cavern roof and the floor increase and the damaged regions propagate further, compared to the baseline case (Figure 11). At the side wall, however, the damage changes little.

Conclusions

Salt cavern storage for natural gas and other hydrocarbons holds several advantages over depleted reservoirs or aquifers, such as higher deliverability, lower cushion gas requirement, lower development cost, and efficiency to initiate the gas flow and refill. In order to maximize storage capacity and deliverability while avoiding cavern closure or collapse, a number of numerical geomechanical models have been developed for single cavern analyses in thin bedded salt.

A baseline model with specified cyclic pressure operations is evaluated in terms of salt stress, deformation, and damage. The salt is described by a modified WIPP-creep viscoplastic model, which includes the WIPP-creep model and Drucker-Prager failure criteria. The non-salt formations are described with a typical Mohr-Coulomb model. Different parameters that affect salt deformation and cavern stability, such as

cavern pressure, operating conditions, cavern size and volume, roof thickness, overburden stiffness, interface properties, etc., are investigated and compared to the baseline study.

The findings are summarized as follows.

- For a single cavern in hydrostatic state, salt deformation primarily distributes around the cavern roof and corners while salt damage is mainly around the cavern wall. The interface slip concentrates at the upper interface between the salt formation and the anhydrite layer. After 1-year cyclic pressure operations, shear stress propagates into a wider area, which is responsible for an increase in the amount of slippage in the interface.
- Hydrostatic pressure results in most stable conditions of the cavern, involving a rather limited amount of damage in the close proximity to the cavern. Lowering the cavern pressure can induce massive damage propagation throughout the entire roof and the cavern floor as well as substantial extension in lateral directions. This demonstrates the most critical operational parameter to cavern stability is the lower pressure limit.
- For a large cavern, the tendency of cavern closure accelerates, and the damaged region and the extension of interface slip increase. The cavern appears "stronger" when its size becomes smaller.
- Thick cavern roof does help improve the cavern stability, particularly near the roof center. But this improvement is not significant along the cavern wall, where most damage concentrates.
- Overburden stiffness is a significant factor in evaluating roof stability of caverns. Soft overburden results in a dramatic increase of the vertical displacement of the cavern roof. This can accelerate interface slip, cavern damage, and may even induce tensile fractures in the anhydrite layer.
- Interface strength, in terms of friction angle, is primarily responsible for how much load can be transferred to the cavern roof. Reducing the interface strength increases the amount and extent of damage to some extent.

These findings improve the understandings of geomechanical behaviors of single cavern in bedded salt. The models developed in this study can provide operators with improved geotechnical design and operating guidelines for thin bedded salt caverns (e.g. maximum and minimum cavern pressure, direct or cyclic pressure draw down, etc).

Acknowledgements

This work was sponsored in part by the Gas Technology Institute through contract GTI 8701 and by the US Department of Energy through contract DE-FC26-03NT41813. Technical discussion with Prof. Maurice B. Dusseault at University of Waterloo is also appreciated.

Nomenclature

DOE Department Of Energy
GTI Gas Technology Institute
H/D Height/Diameter
LNG Liquid Natural Gas

References

1. Donnelly, J.: "The Gas Age", JPT (Dec. 2005) 14.
2. Energy Information Administration: "Natural gas storage in the United States in 2001", http://www.eia.doe.gov/.
3. Bruno, M., Dorfmann, L., Han, G., Lao, K., Young, J.: "3D Geomechanical analysis of multiple caverns in bedded salt", paper presented at the SMRI (Solution Mining Research Institute) 2005 Fall Meeting, Nancy, France, October 2-5.
4. Dusseault, M.B., Maury, V., Sanfilippo, F., and Santarelli, F.J.: "Drilling through salt: constitutive behavior and drilling strategies", paper NARMA/ARMA 04-608, presented at the Gulf Rocks, the 6th North America Rock Mechanics Symposium, Houston, TX, USA, June 5-9.
5. Itasca Consulting Group, Inc.: "FLAC3D Optional Features", 1st edition, Aprl 2002.
6. Pfeifle, T.W., Mellegard, K.D., Senseny P.E: "Preliminary constitutive properties for salt and nonsalt rocks from four potential repository sites", Technical report. RESPEC Inc., July 1983.
7. Fossum, A.F. and Fredrich, J.T.: "Salt mechanics primer for near-salt and sub-salt deepwater Gulf of Mexico field developments", SANDIA Report, SANDIA 2002-2063, July 2002.
8. Senseny P.E.: "Triaxial compression creep tests on salt from the Waste Isolation Pilot Plant", Topical report RSI-0294, 1986.
9. DeVries, K.L., Callahan, G.D., and Mellegard, K.D.: "Numerical simulation of natural gas storage caverns in beded salt", paper ARMA/USRMS 05-734, Alaska Rocks 2005, the 40th US Symposium on Rock Mechanics (USRMS), Anchorage, Alaska, USA, June 25-29.

SI Metric Conversion Factors

ft × 3.048	E-01 = m
ft^3 × 3.6315	E+01 = m^3
lbf × 4.448222	E+00 = N
psi × 6.894757	E+00 = kPa
lb/ft^3 × 6.243	E-02 = kg/m^3

Tables and Figures

Table 1: Geomechanical properties for different formations

Material	Bulk Modulus		Shear Modulus		Density		Tensile Strength		Cohesion		Friction Angle (deg)
	(GPa)	(MPsi)	(GPa)	(MPsi)	(kg/m^3)	(lb/ft^3)	(MPa)	(Psi)	(MPa)	(KPsi)	
Clastic	13.3	1.93	8	1.16	2000	124.86	4	580	15	2.175	35
Anhydrite	100.48	15.0	22.69	3.29	3000	187.28	7	1015	40	5.8	35
Salt	26.08	3.78	10	0.14	2100	131.1	0.4	58	N/A		N/A
Pre-Salt	24.1	3.49	21.6	3.13	2700	168.56	4	580	2	2.9	35

Table 2: Material properties for salt

	SI Unit	Field Unit
WIPP Model Constant A	15.625	
WIPP Model Constant B	210.013	
WIPP Model Constant D	0.286 MPa^{-n} /day	7.365E-12 $1/psi^n$/day
Activation Energy Q	12000 cal/mol	
Steady-State Creep Rate	0.0043 /day	
Gas Constant R	1.987 cal/mol K	
WIPP Model Exponent n	4.9	
Bulk Modulus	26078 MPa	3.78 MPsi
Shear Modulus	10000 MPa	0.14 MPsi
Zone Temperature	31 ^oC	87.8 ^oF
Material Parameter kphi	1.9	
Material Parameter kkappa	0.1	
Material Parameter qphi	0.2	
Tensile Strength	0.4 MPa	58 psi

Table 3: Simulation matrix for single cavern stability analyses

Model Number	H/D Ratio	Cavern Height		Cavern Diameter		Cavern Volume		Roof Thickness		Interface Friction (deg)	Pressure
		(m)	(ft)	(m)	(ft)	($\times 10^3 m^3$)	($\times 10^6 ft^3$)	(m)	(ft)		
1	1/2	30	98.4	60	196.8	84.78	2.992	12	40	15	Cyclic
2	1/4	30	98.4	120	393.6	339.12	11.967	12	40	15	Cyclic
3	1/1	30	98.4	30	98.4	21.2	0.748	12	40	15	Cyclic
4	1/2	30	98.4	60	196.8	84.78	2.992	12	40	15	Hydrostatic
5	1/4	30	98.4	120	393.6	339.12	11.967	12	40	15	Hydrostatic
6	1/1	30	98.4	30	98.4	21.2	0.748	12	40	15	Hydrostatic
7	1/2	30	98.4	60	196.8	84.78	2.992	12	40	15	Pressure Drawdown
8	1/4	30	98.4	120	393.6	339.12	11.967	12	40	15	Pressure Drawdown
9	1/1	30	98.4	30	98.4	21.2	0.748	12	40	15	Pressure Drawdown
10	1/2	30	98.4	60	196.8	84.78	2.992	24	80	15	Cyclic
11	1/2	30	98.4	60	196.8	84.78	2.992	12	40	15	Cyclic
12	1/2	30	98.4	60	196.8	84.78	2.992	12	40	5	Cyclic

Figure 1: Major salt deposits and dry salt production sites in North America (source: the Salt Institute)

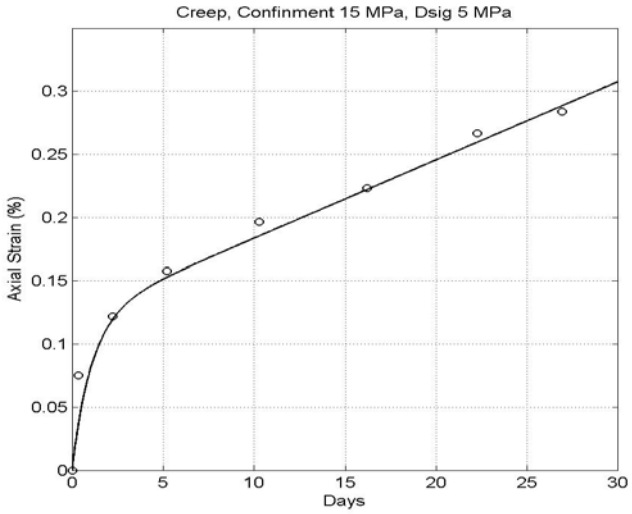

Figure 2: Creep response of a salt model (circles are from lab data[5], line is from the numerical model)

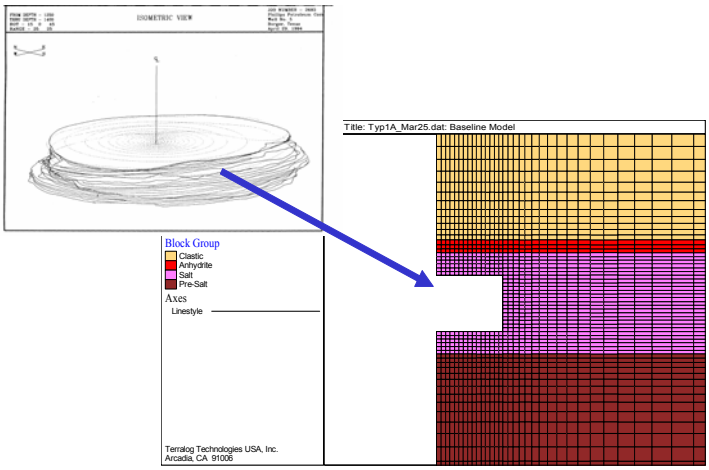

Figure 3: Geomechanical model for single bedded salt caverns (from top to bottom: clastic, anhydrite, salt, and pre-salt layers)

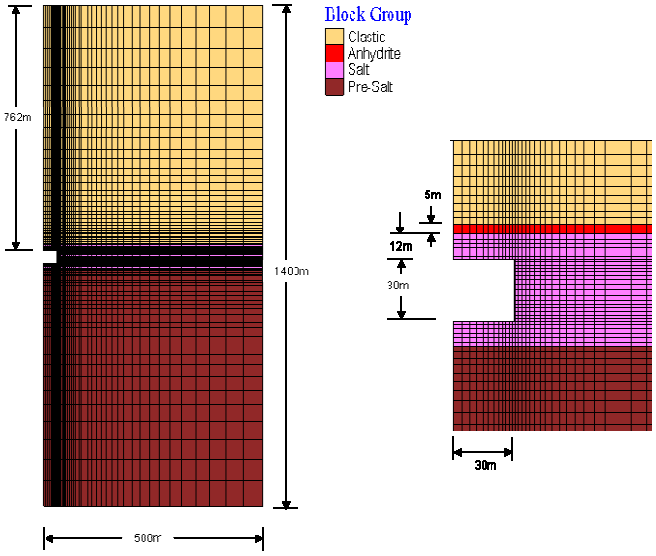

Figure 4: Model configurations for baseline study

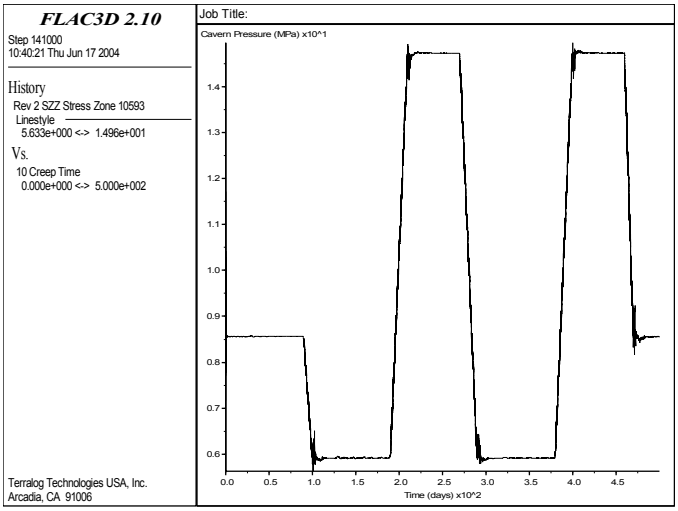

Figure 5: Simulated pressure cycles in the cavern for 1 year

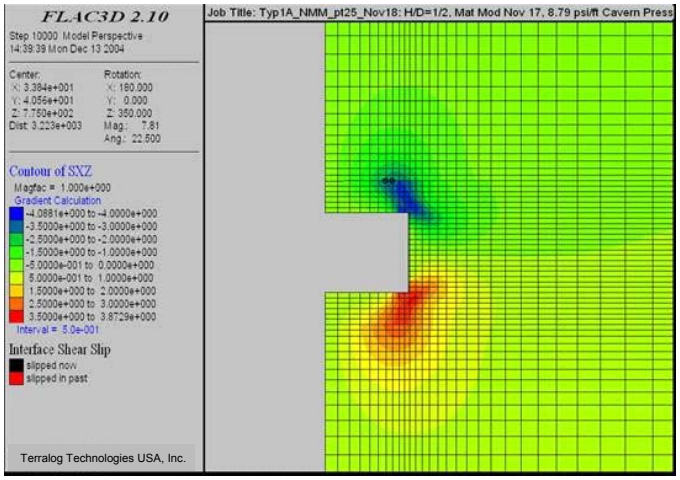

Figure 6: Shear stress and interface slip (circles) in baseline model at 8.8MPa (1276psi) hydrostatic cavern pressure

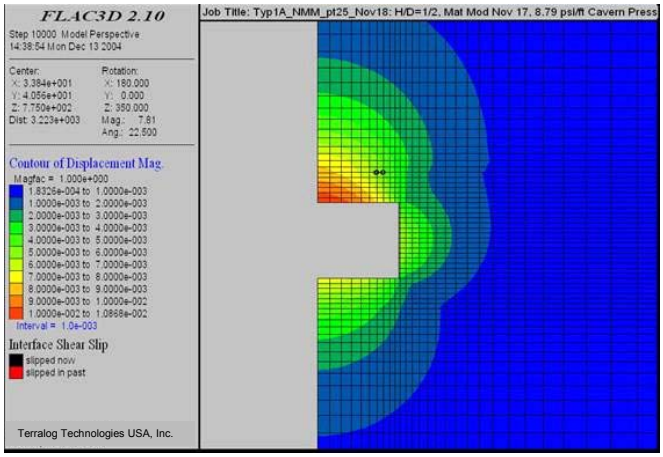

Figure 7: Rock displacement around cavern at 8.8MPa (1276psi) hydrostatic pressure

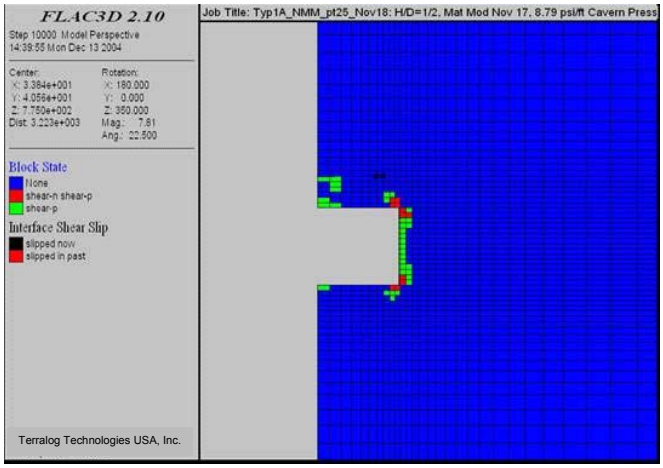

Figure 8: Micro-cracks developed around cavern after 8.8MPa (1276psi) hydrostatic pressure

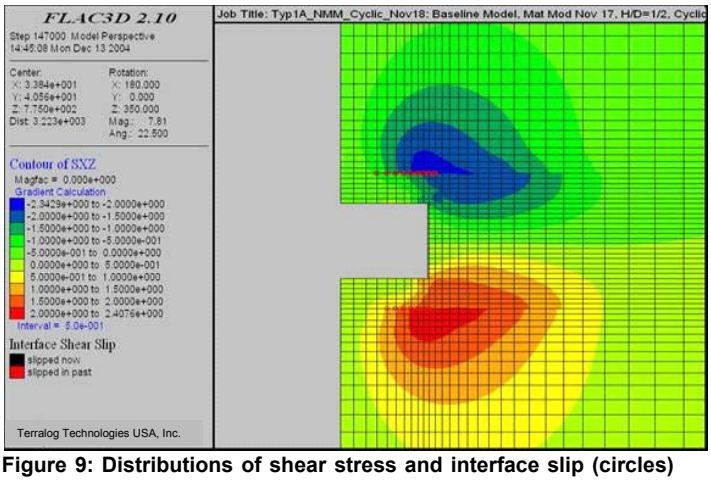

Figure 9: Distributions of shear stress and interface slip (circles) around cavern after 1 year pressure cycles

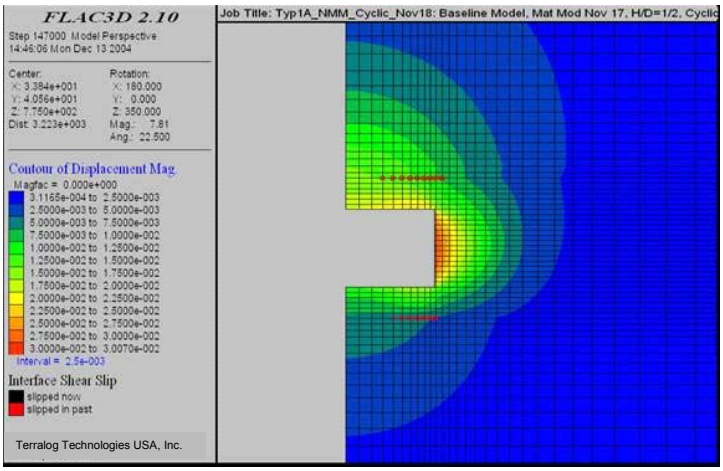

Figure 10: Rock displacement around cavern after 1 year pressure cycles

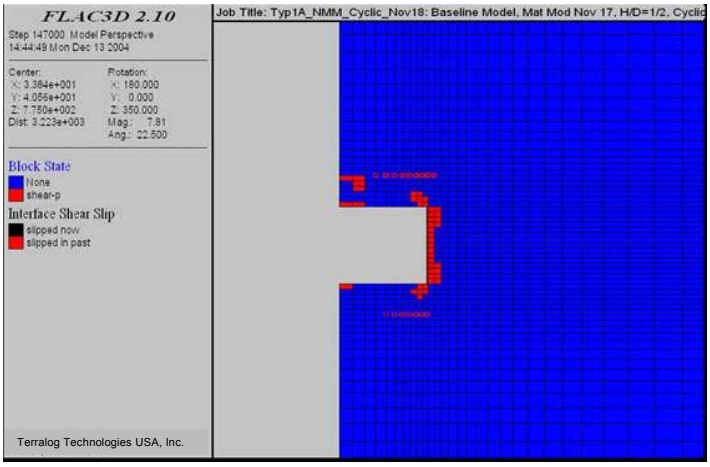

Figure 11: Development of micro-cracks around cavern after 1 year pressure cycles

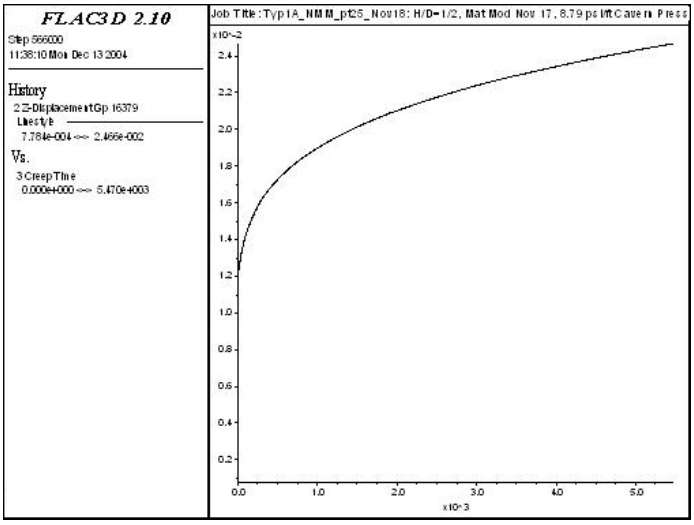

Figure 12: Vertical displacement of the cavern roof over 15 year. Cavern pressure is constant and equal to 8.8 MPa (1276 psi).

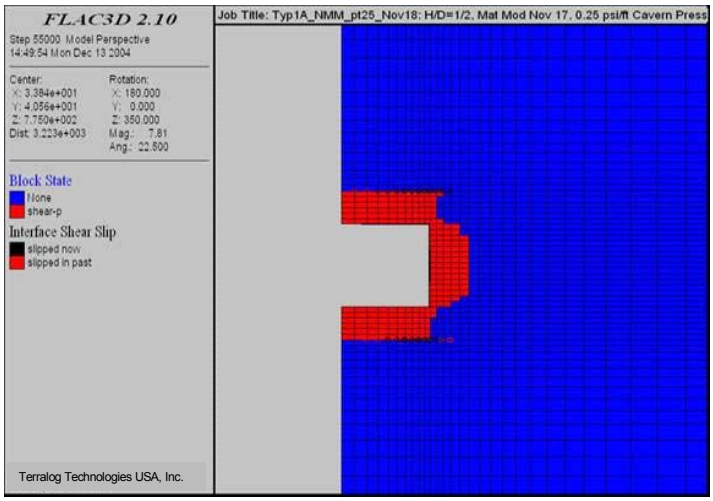

Figure 13: Propagation of Micro-cracks around the cavern after 1 year direct pressure drawdown to 4.4MPa (638psi)

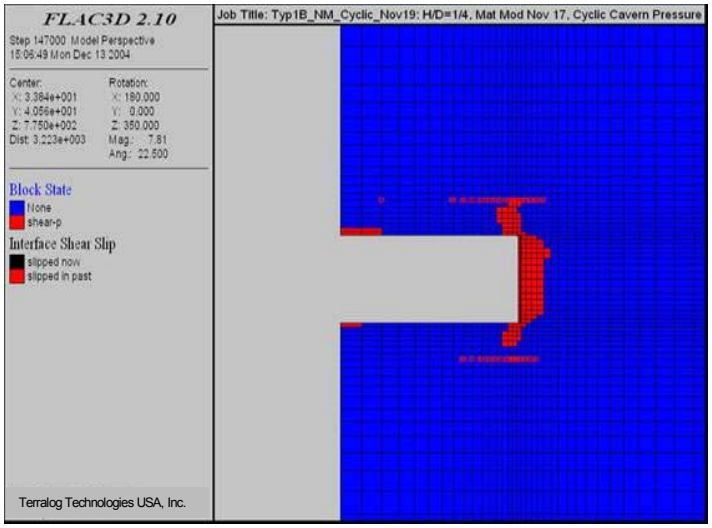

Figure 14: Distribution of micro-cracks around a cavern with H/D=1/4 after 1 year pressure cycles

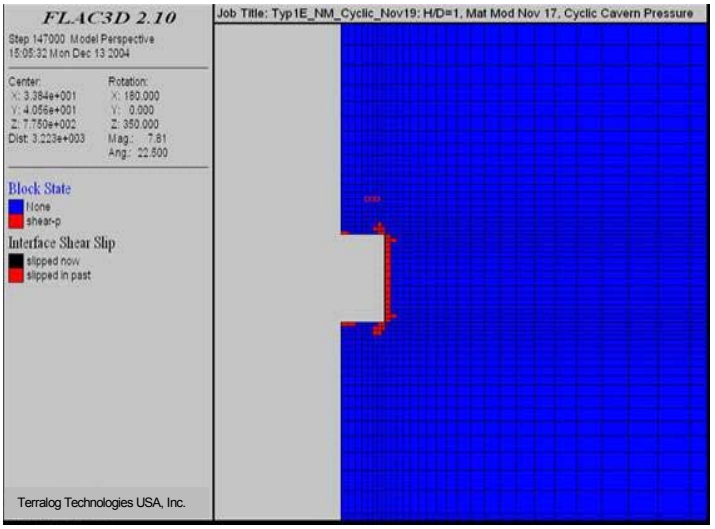

Figure 15: Distribution of micro-cracks around a cavern with H/D=1 after 1 year pressure cycles

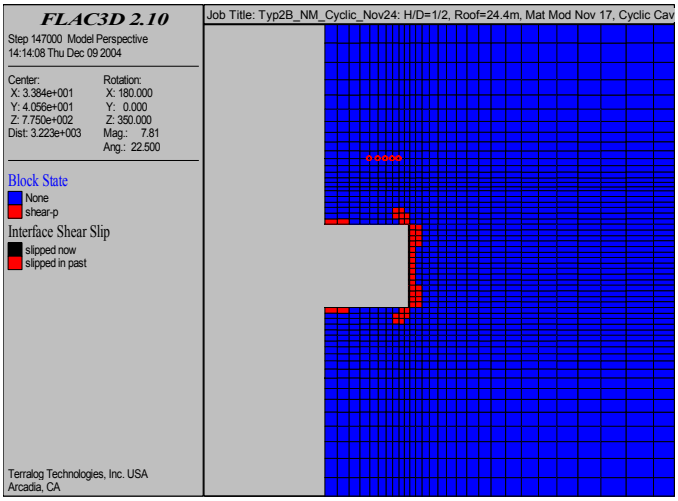

Figure 16: Distribution of micro-cracks around a cavern with double roof thickness after 1 year pressure cycles

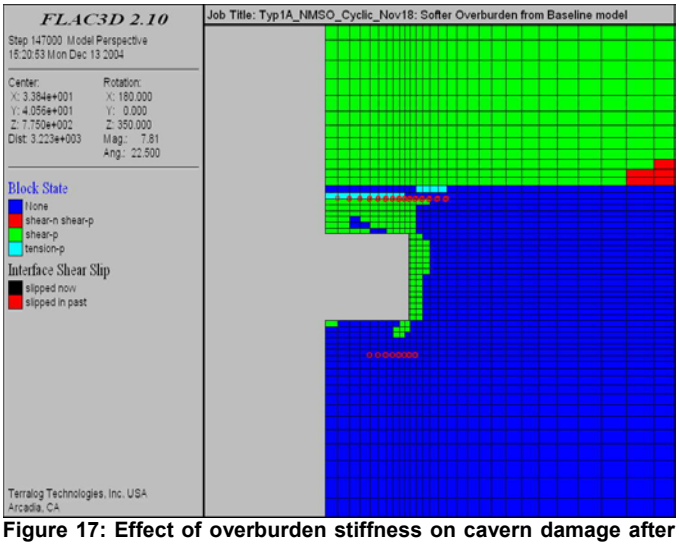

Figure 17: Effect of overburden stiffness on cavern damage after 1 year pressure cycles

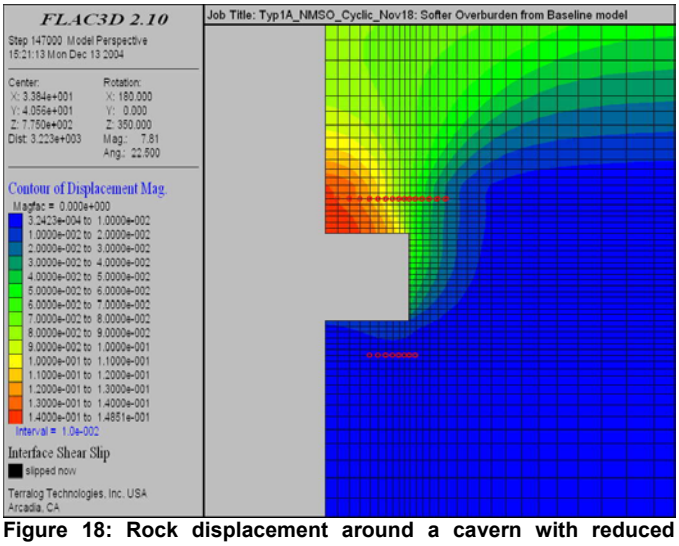

Figure 18: Rock displacement around a cavern with reduced overburden stiffness

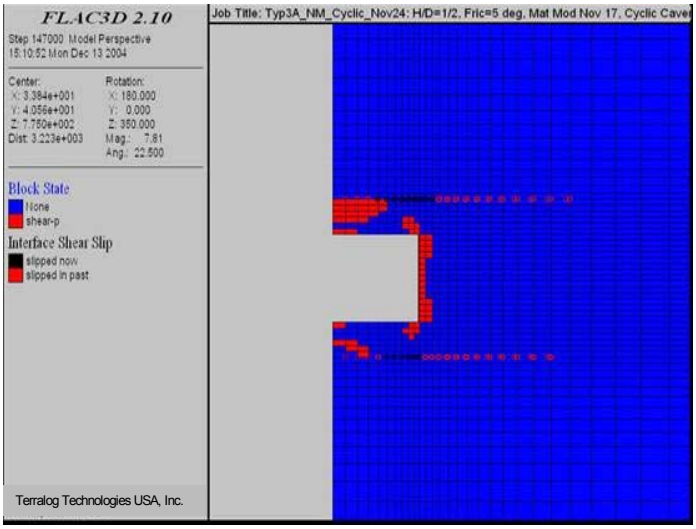

Figure 19: Distribution of micro-cracks and interfacial slip around a cavern with softer interface properties (friction angle reduced from 35 to 5 degree)